Journal Pre-proofs

Lyotropic liquid crystal emulsions of LAVR-289: Influence of internal mesophase structure on cytotoxicity and *in-vitro* antiviral activity

Mathias Brouillard, Thomas Mathieu, Samuel Guillot, Fabienne Méducin, Vincent Roy, Elie Marcheteau, Franck Gallardo, François Caire-Maurisier, Patrick Favetta, Luigi A. Agrofoglio

Please cite this article as: M. Brouillard, T. Mathieu, S. Guillot, F. Méducin, V. Roy, E. Marcheteau, F. Gallardo, F. Caire-Maurisier, P. Favetta, L.A. Agrofoglio, Lyotropic liquid crystal emulsions of LAVR-289: Influence of internal mesophase structure on cytotoxicity and *in-vitro* antiviral activity, *International Journal of Pharmaceutics* (2024), doi: https://doi.org/10.1016/j.ijpharm.2024.124683

This is a PDF file of an article that has undergone enhancements after acceptance, such as the addition of a cover page and metadata, and formatting for readability, but it is not yet the definitive version of record. This version will undergo additional copyediting, typesetting and review before it is published in its final form, but we are providing this version to give early visibility of the article. Please note that, during the production process, errors may be discovered which could affect the content, and all legal disclaimers that apply to the journal pertain.

Lyotropic Liquid Crystal Emulsions of LAVR-289: Influence of Internal Mesophase Structure on Cytotoxicity and *In-vitro* Antiviral Activity

Mathias Brouillard[a], Thomas Mathieu[a], Samuel Guillot[b,*], Fabienne Méducin[b], Vincent Roy[a], Elie Marcheteau[c], Franck Gallardo[c], François Caire-Maurisier[d], Patrick Favetta[a,*], Luigi A. Agrofoglio[a,*]

[a] Institut de Chimie Organique et Analytique (ICOA UMR 7311), Université d'Orléans, CNRS, F-45067 Orléans, France

[b] Interfaces, Confinement, Matériaux et Nanostructures (ICMN UMR 7374), Université d'Orléans, CNRS, F-45071 Orléans, France

[c] NeoVirTech, SAS, F-31106 Toulouse, France

[d] Direction des Approvisionnements en produits de Santé des Armées, Pharmacie Centrale des Armées (PCA), F-45404 Fleury-les-Aubrais, France

Abstract

Emerging and reemerging viruses pose significant public health threats, underscoring the urgent need for new antiviral drugs. Recently, a novel family of antiviral acyclic nucleoside phosphonates (ANP) composed of a 4-(2,4-diaminopyrimidin-6-yl)oxy-but-2-enyl phosphonic acid skeleton (*O*-DAPy nucleobase) has shown promise. Among these, LAVR-289 stands out for its potent inhibitory effects against various DNA viruses. Despite its efficacy, LAVR-289's poor water solubility hampers effective drug delivery. To address this, innovative delivery systems utilizing lipidic derivatives have been explored for various administration routes. Submicron lyotropic liquid crystals (LLCs) are particularly promising drug carriers for the encapsulation, protection, and delivery of lipophilic drugs like LAVR-289.

This study focuses on developing submicron-sized lipid mesophase dispersions, including emulsified L_2 phase, cubosomes, and hexosomes, by adjusting lipidic compounds such as Dimodan® U/J, Lecithins E80, and Miglyol® 812N. These formulations aim to enhance the solubility and bioavailability of LAVR-289. *In vitro* evaluations demonstrated that LAVR-289-loaded LLCs at a concentration of 1 μM efficiently inhibited vaccinia virus in infected human cells, with no observed cytotoxicity. Notably, hexosomes exhibited the most favorable antiviral outcomes, suggesting that the internal mesophase structure plays a critical role in optimizing the therapeutic efficacy of this drug class.

Keywords

Lyotropic Liquid Crystals; Lipid Mesophase; Drug Delivery System; Lipophilic Drug; Antiviral acyclic nucleoside phosphonate

1. Introduction

Internally structured lipid nanocarriers have emerged as powerful tools for delivering highly lipophilic and metabolically unstable drugs, significantly enhancing their efficiency.[1] These carriers possess diverse compositions, optimized surface-to-volume ratios, improved stability, and flexible properties, rendering them promising systems for delivering a range of therapeutics, including antivirals, as well as imaging and

diagnostic agents.[2] Despite the high *in vitro* activities of new pharmaceutical compounds, their development is often hindered by poor solubility, limited stability, or variable bioavailability, impeding the advancement of novel antiviral drugs.[3] For the acyclonucleoside phosphonate antiviral family, including the recently developed LAVR-289 (**Figure 1**),[4] low bioavailability—whether administered orally or topically—substantially limits their therapeutic efficacy.[5]

To address these issues, recent decades have seen the increasing use of innovative antiviral delivery systems, such as lipid-based technologies, to formulate new active pharmaceutical ingredients and reposition discontinued drugs with pronounced adverse side effects.[6] Due to its apolar group structure, this new molecule LAVR-289 exhibits very poor water solubility, classifying it as class II in the Biopharmaceutical Classification System.[7] This characteristic makes it an ideal candidate for solubilization within the lipidic internal nanosystem phase.[8]

Among the available nanosystems, lyotropic liquid crystals (LLC) stand out as promising drug carriers in their dispersed form. The thermodynamically stable lipidic mesophases, which are intermediates between solids and liquids, are being actively investigated for efficient drug delivery and biomedical applications.[9] These stable colloids with nanometric structures are suitable for clinical applications involving hydrophilic, hydrophobic, or amphiphilic molecules through various administration routes, including intravenous injection, oral, topical, or ocular administrations.[10,11,12] The advantages of these systems include enhanced chemical and enzymatic stability, improved intravenous tolerance, increased bioavailability, and versatility, rendering them ideal for delivering the poorly water-soluble antiviral LAVR-289.[13]

Lipid mesophase dispersions, in contrast to liposomes or simple nanoemulsions, offer a significantly larger interfacial area, enabling greater drug payloads and enhances the protection of therapeutics from degradation. For instance, cubic mesophase dispersions can present an interfacial area of approximately 400 $m^2.g^{-1}$,[14,15] least eight times larger than nanoemulsions and forty times greater than liposomes. The latter have a much lower surface area due to their simpler bilayer structure. The intricate internal structure of mesophase dispersions allows for increased drug payloads.

Various mesophase types can be emulsified, including bicontinuous cubic networks,[16] sponge phases,[17] hexagonal phases of water nano-channels,[18] reverse micelles organized in a cubic arrangement,[19] or the L_2 phase.[20,21] The type of emulsified mesophase significantly affects the vectorization process, particularly the release profile of hydrophilic molecules, which depends on whether the water domains inside the mesophase are continuous or discontinuous. Additionally, internalization processes are influenced by the internal structure of the lipid nanocarriers.[22] The nanostructure can be fine-tuned through appropriate additives and careful adjustments to the lipid/water composition. Monoglycerides, such as glyceryl monooleate, and phytantriol have been widely used to develop and tune such systems.[22] Despite the advantages of monoglyceride-based systems, their susceptibility to hydrolysis at the ester bond and oxidation of the unsaturated hydrocarbon bonds presents long-term stability and biocompatibility challenges. Biocompatibility concerns include the potential for hemolysis when administered intravenously.[23] To overcome these drawbacks, biocompatible and stable medium-chain triglycerides (MCT) were used as the main component of the oily phase, considerably reducing the amount of monoglycerides used.

This study aims to optimize formulations for the topical, oral, and intravenous delivery of LAVR-289. The developed lyotropic liquid crystalline formulations with various internal mesophase structures were characterized using Small-Angle-X-ray Scattering (SAXS). Further analysis included particle size distribution, ζ-potential, and stability over time, followed by *in vitro* cytotoxicity and antiviral activity assessments. Thus, this work highlights the correlation between the intrinsic structural properties of these mesophase dispersions and their biological responses, providing insights into the potential of LLCs as effective lipophilic drug delivery systems for antiviral therapies.

2. Material and methods
2.1. Material

The active antiviral molecule LAVR-289 (**Figure 1**), (*Z*)-2-[(2,6-diaminopyrimidin-4-yl)oxymethyl]-4-[3-hexadecoxypropoxy (isopropoxycarbonyloxy-methoxy)phosphoryl]but-2'-enyl] acetate, was synthesized as

previously described.[24] Compounds for mesophase dispersion compositions were used as received. Dimodan® U/J (DU), a commercial-grade form of monolinolein, was used as the structuring lipid. This was kindly supplied by Danisco A/S (Brabrand, Denmark) and consists of 96% distilled monoglycerides (62% monolinoleates). Medium-chain triglycerides (Miglyol® 812N) and egg lecithin (Lipoid® E80) were generously provided by IOI Oleo GmbH and Lipoid GmbH, respectively. Steric stabilization of the dispersions was achieved using the emulsifier triblock copolymer Pluronic F127 (PEO$_{99}$-PPO$_{67}$-PEO$_{99}$). Both F127 and Tween 80 were supplied by Sigma Aldrich.

LAVR-289
Chemical Formula: C$_{35}$H$_{63}$N$_4$O$_{10}$P
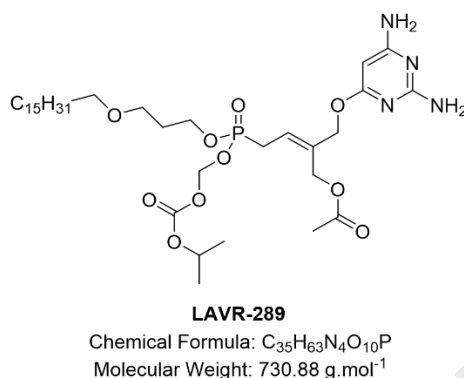Molecular Weight: 730.88 g.mol^{-1}

Figure 1: Molecular structure of LAVR-289.

2.2. LogP determination of LAVR-289

The LogP value of LAVR-289 was determined using the reversed-phase chromatography method,[25] with a Kromasil® C18 column (100 x 2.1 mm, 3.5 μm). The octanol/water partition coefficient affects the retention time since hydrophilic molecules elute first, while lipophilic ones are retained longer. A total of twenty-four standard chemical compounds were injected at a flowrate of 0.5 mL/min in a MeCN/H$_2$O (75/25, v/v) mobile phase (**Table S1**). The capacity factor is defined by the retention time as $k = \frac{t_R - t_0}{t_0}$, where t_R is the retention time of the substance and t_0 is the dead-time. A linear regression was established by plotting the substances' log k values versus their known LogP values obtained from pubchem.ncbi.nlm.nih.gov. The LogP value of LAVR-289 was then determined using the equation $\log P_{OW} = a + b \times \log k$.

2.3. Lipid mesophase dispersion preparation

Reversed mesophase dispersions were formulated using medium-chain triglycerides (MCT) and varying lipid fractions in a 1 g final mixture. All mixtures were dispersed by keeping the oily weight ratio constant at about 8%. Aqueous dispersions were prepared with different additive contents, defined by the mass ratio $\delta = 100 \times DU/(DU+additive)$. Additives can be MCT or MCT/LE80 mixtures. In the case of mixtures of additives, the ratio $\alpha = 100 \times LE80/(LE80+MCT)$ represented the mass fraction of lecithin E80 (LE80) substituting MCT in the total mass of additives.

To produce literature-based nanoemulsions, the oily phase was composed of 12 mg egg LE80 dispersed in 200 mg Miglyol® 812N, while the aqueous phase contained 25 mg polysorbate 80 (Tween® 80) in 800 mg Milli-Q water, as previously reported.[26] To prepare α5 to α100 dispersions, the oily phase consisted of egg LE80 dispersed in MCT, along with monoglycerides (Dimodan®), while the aqueous phase consisted in Pluronic® F127 dispersed in Milli-Q water. Adjustments to α fine-tuned the internal emulsion structure. The emulsification process involved heating both the aqueous and oily phases to 70 °C, followed by ultrasonic dispersion for 7 min at 30% of maximum power in a 1s on/1s off pulse mode (Ultrasonic liquid processor VCX 750 from SONICS, 750W power supply, with an ultrasound tip working at 20 kHz). This procedure ensured the integrity of LAVR-289 and prevented substantial lipid degradation.[27] For loaded dispersed lipid mesophases, LAVR-289 was solubilized in the oily phase before mixing. α0 to α75 compositions at δ85,

3

expressed in % w/w, are detailed in **Table 1**. All formulations are detailed in the supporting information section (**Table S2)**.

Table 1: Compositions of loaded lyotropic liquid crystalline emulsions with LAVR-289

Composition	% w/w
LAVR-289	0.1%
Dimodan®	3.93%
Lipoid® E80	0 - 0.17%
Miglyol® 812N	0.55 - 0.69%
Pluronic® F127	0.38%
H$_2$O *qs*	100%

2.4. ¹H and DOSY NMR analysis

NMR analysis of mesophase dispersions was performed at 298 K on a Bruker Avance III HD 700-MHz NMR spectrometer equipped with a 5-mm TCI cryoprobe, using residual D$_2$O as an internal reference (4.79 ppm). Data processing was carried out using Bruker's TopSpin 3.6 and MestreNova 14.2.0 software. 2D Diffusion Ordered Spectroscopy (DOSY) sequence, for diffusion measurement, used stimulated echo (stebpgp1s19), bipolar gradient pulses with 100 ms diffusion delay, 1 spoil gradient water suppression using 3-9-19 pulse sequence with gradient duration 5 ms, and a relaxation delay of 8 s.

2.5. Nanosystems characterization

Dispersed lipid-based mesophases were characterized by Small-Angle-X-ray Scattering (SAXS). Experiments were conducted using a Xeuss SAXS/wide-angle X-ray scattering system from Xenocs. The instrument features a GeniX 3D MicroSpot source operating at 50 kV and 0.6 mA, providing an X-ray beam with a photon wavelength of $\lambda = 0.1541 \, nm$ (Cu Kα radiation). The scattered intensity as a function of the length of the scattering vector $q = 4\pi \, sin(\theta/2)/\lambda$, with θ being the scattering angle, was recorded on a 2D detector (Pilatus 300K, Dectris) with a sensitive area of 83.8 x 106.5 mm² and a pixel size of 172 x 172 μm². The sample-detector distance of 1.170 m allowed coverage of a scattering q range of 0.1-4.3 nm⁻¹. SAXS profiles were recorded for 8 hours at 22 °C using cylindrical capillaries with a 1 mm diameter

4

(Hilgenberg). Indexing of the Bragg peak positions enable the determination of the internal mesophase within the droplets, the space group, and the mean lattice parameter: $a = 2\pi\sqrt{h^2+k^2+l^2}/q_{hkl}$ for cubic structures or $a = 4\pi\sqrt{h^2+hk+k^2}/(q_{hk}\sqrt{3})$ for 2D-hexagonal structures, where h, k, and l are the Miller indices. For profiles exhibiting a broad correlation peak (*e.g.*, L_2 phase), the characteristic distance $a = 2\pi/q_0$ was deduced from the peak position q_0 at maximum intensity.

Granulometric profiles and hydrodynamic droplet mean diameter were assessed by dynamic light scattering (DLS) using a Zetasizer Nano ZS90 (Malvern Instruments). Data were obtained from three independent measurements on samples diluted by a factor of 2,000 to avoid multiple scattering effects. Measurements were performed at 25 °C, with a wavelength of 633 nm, and a fixed scattering angle of 90°. At this dilution, the solvent viscosity was assumed to be equivalent to that of water. Each measurement consisted of an average of 11 runs. ζ-potential values were measured on a Zetasizer Nano ZS coupled with a folded capillary cell (DTS1060) from Malvern Instruments.

2.6. HPLC method

Formulations were analyzed with an HPLC system to verify LAVR-289 stability. All mixtures were analyzed using an Agilent 1260 Infinity HPLC chromatograph (Agilent Technologies, Les Ulis, France). The chromatograph was equipped with a 1260 binary pump (G1311B), a 1260 standard autosampler (G1329B), a 1260 thermostated column compartment (G1316A), and a 1260 diode array detector (G4212B) with a Max-Light cartridge cell (1 µL volume, 10 mm cell path length). A Poroshell 120 Bonus-RP column (150 × 2.1 mm, 2.7 µm particle size) with a UHPLC guard column Poroshell 120 Bonus-RP (5 x 2.1 mm, 2.7 µm) (Agilent Technologies, Les Ulis, France) was used. The injection volume was 1 µL, and the column oven was maintained at 40 °C. Separation of LAVR-289 from other compounds in the formulations was achieved using isocratic elution with acetonitrile/water (72/28, v/v) at a flow rate of 0.3 mL/min. The UV wavelengths for plotting the chromatogram were set to the maximum absorbance of LAVR-289 at 267 nm and the maximum absorbance of the major degradation product of LAVR at 230 nm.

2.7. Cell culture

HeLa (human cervical cancer cells) were cultured in Dulbecco's modified Eagle's medium (DMEM; Thermo Fisher Scientific, Illkirch, France) 4.5 g/L glucose, 2 mM glutamine containing 10% fetal bovine serum (FBS, Eurobio), 100 IU/mL penicillin, and 100 µg/mL streptomycin (Thermo Fisher Scientific). Cells were incubated at 37 °C with 5% CO_2.

2.8. In vitro cytotoxicity and antiviral activity

HeLa cells were cultured at 10,000 cells per well in a 96-well plate (Corning Cell Bind) in 200 µl DMEM without phenol red. At day 1, cells were treated with unloaded and drug-loaded formulations (ranging from 10 to 0.01 µM in 10-fold serial dilution) in triplicate and immediately infected using VACV ANCHOR™ at a multiplicity of infection (MOI) of 0.1. 48 hours post-infection, cells were fixed with formalin for 10 min at room temperature, washed with 200 µL PBS, and stained with 100 µL PBS/Hoechst 33342 per well. The 96-well plates were stored at 4 °C and protected from light until data acquisition. Image acquisition and high-content data analysis were performed on a Thermo CellInsight CX7 microscope using a modified compartmental analysis algorithm. Cell toxicity was assessed by determining the number of cell nuclei per condition normalized to the untreated control. The infection rate was determined by the number of ANCHOR-positive cells relative to the total number of cells, normalized to untreated conditions.

2.9. Statistical analysis

The data's statistical significance was assessed in GraphPad Prism® software through a one-way or two-way analysis of variance (ANOVA), followed by Tukey's multiple comparison test. The significance level was set at $p < 0.05$.

3. Results and discussion

3.1. LogP determination of LAVR-289

To develop an optimized vehicle for encapsulating, protecting, and delivering the antiviral of interest, determining the LogP was an essential step. The partition coefficient (LogP) represents the equilibrium concentration ratio of a solute in two immiscible solvents (typically *n*-octanol and water). Given the structure of LAVR-289, high lipophilicity was expected. However, precise measurement was necessary for defining the optimal drug delivery system. To measure the LogP of LAVR-289, a reversed-phase chromatography method was developed by plotting Log k against LogP values of various compounds (**Table S2**). This approach estimated LAVR-289 LogP to be 7.33 (**Figure S1**), which is in close agreement with the *in-silico* calculation of 7.38 from Marvin Sketch® software. This particularly high value indicates a strong tendency to be soluble in fat-like solvents.

3.2. Nanosystems compositions

The pronounced lipophilicity of LAVR-289 makes it an ideal candidate for lipid-based delivery systems like LLC, which enhance bioavailability by promoting cellular permeability. Therefore, the development of lipid-based drug delivery systems was prioritized, specifically focusing on developing various internal formulation structures to enhance biological activities. Initially, a biocompatible formulation from the literature, with FDA-approved components, comprising medium-chain triglycerides (MCT) and lipidic emulsifiers was selected. This formulation, known for encapsulating nucleoside analogs,[28] is suitable for small-scale processing – a crucial criterion for this work's scope. Furthermore, this composition enabled the efficient transport of active drugs and remained stable for months**Error! Bookmark not defined.**.[29] The chosen solubilizing oil is biocompatible and versatile, supporting various administration routes, including oral administration, parenteral injection, intramuscular administration, and topical applications. Additionally, these nanosystems could be tailored for pulmonary administration to target respiratory tract infections or brain damage.[14,27]

To further explore the behavior of LAVR-289 in lipid environments, dispersions containing MCT, LE80, and polysorbate as emulsifiers were prepared. The SAXS profile (**Figure S2**) revealed that the emulsion system formed a nanoemulsion without any specific structure in the dispersed phase. Therefore, to induce internal structuring, monolinolein (DU) was incorporated, and lipid ratios were modified. While this approach generated short-lived structures, the system lost its integrity too quickly to allow a full evaluation of how the lipid ratios adjustments affected the mesophase organization. Consequently, an efficient stabilizing block copolymer was added to enable further study of DU's impact on dispersion behavior.

3.3. Characterization of DU/MCT/LE80 dispersions

The internal structure of lipid-based aqueous dispersions can be significantly affected by additives such as the hydrophobic surfactant DU. To explore various lipid-based nanostructures, mixtures of DU and MCT were emulsified at varying δ ratios. **Figure 2** presents SAXS profiles obtained at δ0 and within the δ50-100 range.

In the absence of MCT (δ100), DU-based dispersions stabilized by F127 exhibited bicontinuous cubosomes, characterized by an internal structure of the Im3m type. This structure was identified by a set of eight distinct Bragg peaks with spacing ratios of $\sqrt{2}:\sqrt{4}:\sqrt{6}:\sqrt{10}:\sqrt{12}:\sqrt{14}:\sqrt{18}:\sqrt{22}$. These particles, containing a bicontinuous cubic mesophase, consist of well-organized lipid bilayers. Conversely, at δ0 (no DU), the scattered intensity as a function of *q* showed an expected pattern from an oil-in-water (O/W) emulsion, indicating that complete substitution of DU by MCT resulted in structureless colloids.

When the lipid ratio was adjusted between 50 to 95, SAXS patterns displayed a broad peak, as observed in samples at δ95, 70, and 50 (**Figure 2**), suggesting a less organized mesophase than the cubic one, likely an L_2 phase. All dispersions produced with the addition of MCT to DU resulted in emulsified L_2 phase (ELP). The transition from the bicontinuous cubic mesophase Im3m to an ELP occurred with as little as 5% MCT, highlighting the strong impact of MCT on promoting highly negative curvatures at the DU/water interfaces. This effect was due to the large hydrophobic tail volume formed by the three aliphatic chains of MCT's caprylic/capric triglycerides. Unlike other triglycerides that promote reverse hexagonal mesophases in monolinolein/water systems, the combination of MCT and DU only yielded ELPs.[30] Granulometric profiles of these systems are available in the supporting information (**Table S3**).
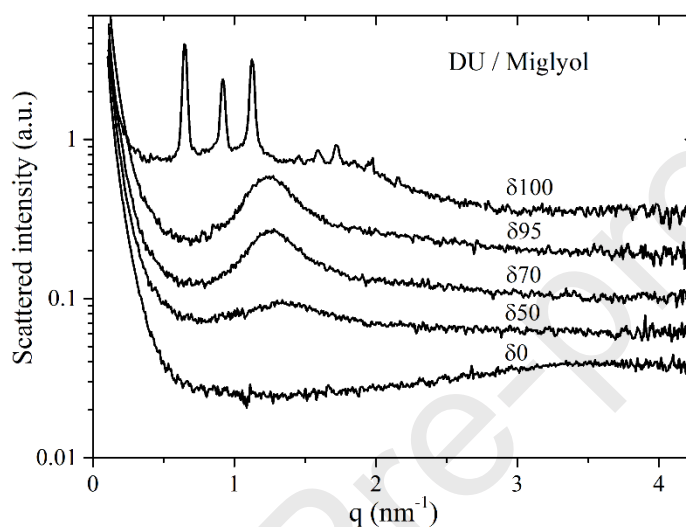

Figure 2: SAXS profiles of DU/MCT/water dispersions stabilized by F127 at selected contents of MCT. The curves were shifted for better visibility.

The influence of MCT on the lipid/water system is further evidenced by a slight decrease in the characteristic distance within the L_2 phase as the DU/MCT ratio decreases (**Figure 3**). As previously mentioned, MCT had an interface-tuning effect, promoting more negative mean curvatures. This geometric effect resulted in smaller sizes of the water domains within the L_2 phase, lowering the characteristic distance, as observed in **Figure 3**. The decreasing intensity level at the broad peak apex upon the addition of MCT reflects a strong decrease in the amount of water in the particles. Notably, the low relative peak intensity at δ50 underlines the substantial impact of MCT on the internal structure of the emulsion droplets. Since the transition toward simple emulsions occurred at larger δ values than with other hydrophobic additives, further characterization of DU/MCT mixtures below δ50 was unnecessary.
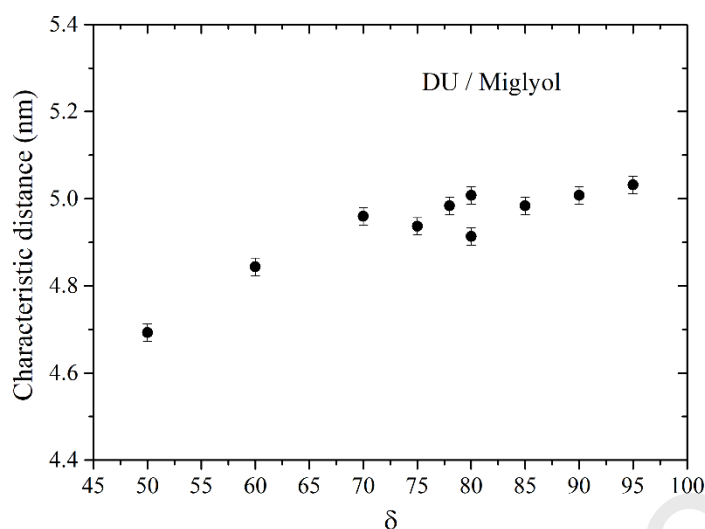
7

Figure 3: Evolution of the characteristic distance of the dispersed L_2 phase of DU/MCT/water mixtures as a function of the MCT content (to δ80, 2 samples are made).

To explore different mesophases for the encapsulation of LAVR-289, an additional component was introduced into the dispersed material. The aim was to identify at least one other mesophase besides the bicontinuous cubic phase or an ELP. Phospholipids (LE80) were incorporated into the DU/MCT mixtures while maintaining the DU content at 85 wt% of the dispersed phase. Various attempts were carried out to generate colloids with different LE80/MCT ratios, totaling 15 wt% of the dispersed phase, with the α ratio representing the percentage of LE80 in the additives' mixture.

Initially, the dispersion of DU/MCT at δ85 consisted in ELP droplets. SAXS patterns from this ELP to new dispersions with varying α are shown in **Figure 4**. For α values above 50, the DU/MCT/LE80 mixtures could not be dispersed as stable emulsified systems, resulting in a significant deposit at the bottom of the vial. For $\alpha \leq 50$, all dispersions produced when MCT was partially replaced by LE80 exhibited an internal reverse hexagonal phase (H_2). This structural transformation from ELP to hexosomes occurred with as little as 5% of LE80 out of the 15% of additives. Thus, LE80 had a counter effect compared to MCT. The addition of LE80 tuned the internal DU/MCT structure from the L_2 to H_2 phases, but only within a narrow range of LE80 contents. This structural effect can be attributed to the presence of phosphatidylcholine, which contains two hydrophobic tails favoring the formation of lipid bilayers, *i.e.*, systems with nearly zero mean curvature interfaces. MCT imposed strong negative DU/water interfacial curvatures, counteracted by the presence of a small amount of phospholipids.
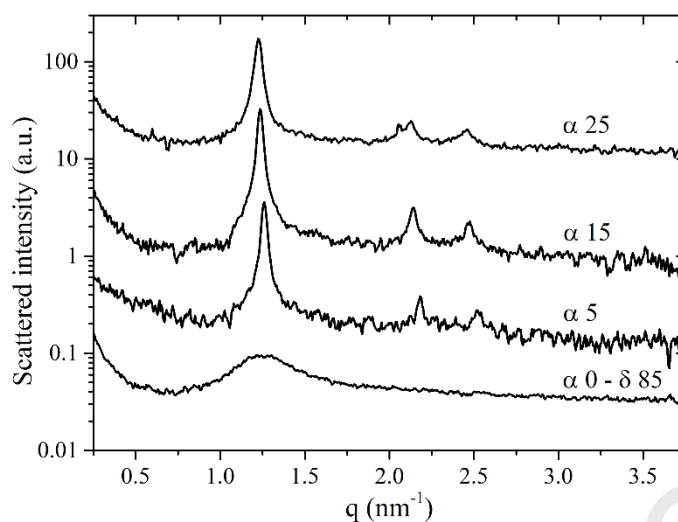
Figure 4: SAXS profiles of blank dispersions at δ85 by varying the LE80/MCT α ratio. Scattered profiles were shifted for better visibility.

As the LE80/MCT α ratio increased from 5 to 25, a slight continuous increase in the hexagonal lattice parameter was measured (**Figure 5**). This result aligned with the tuning-back effect of LE80 on the mean interface curvatures, where larger water domains expanded the lattice parameter. It is worth noting that the DU/LE80/MCT/F127 mixture did not consistently yield stable and homogeneous dispersion. A minimum quantity of MCT was required to achieve a successful formulation and obtain the expected hexagonal phase.
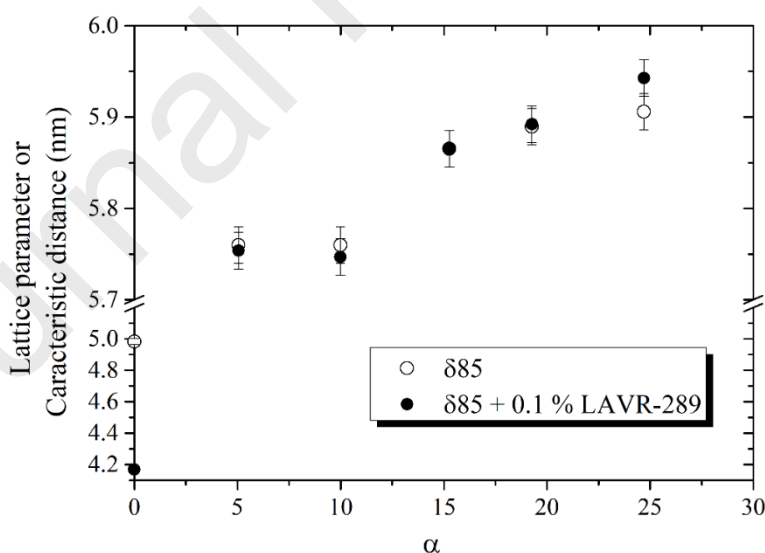

Figure 5: Comparison of lattice parameters (H_2) and characteristic distances (L_2 at $\alpha 0$) of blank emulsions and dispersions containing 0.1% of LAVR-289 by varying the α LE80/MCT ratio.

3.4. Incorporation effects of LAVR-289 in DU/MCT/LE80 mesophases

The SAXS patterns for the three selected mesophases doped with LAVR-289 are presented in **Figure 6**. In the case of the blank bicontinuous cubic phase (δ100), incorporating LAVR-289 at only 0.1% (w/w) dramatically altered the dispersed particles. The scattered intensity exhibited two peaks in a 1:2 ratio,

9

indicative of lamellar symmetry with a repeating distance of 4.22 nm (**Figure 6A**). Consequently, bicontinuous cubosomes could not incorporate the drug, resulting in the formation of multilamellar vesicles. As a result, the size and size distribution of the dispersion were much larger compared to other miniemulsions (**Table S3**).

In contrast, hexosomes remained largely unaffected by the addition of 0.1% LAVR-289. As illustrated in **Figure 5**, the hexagonal lattice parameters remained unchanged for all dispersed mixtures containing LE80, regardless of the presence of the drug. Thus, this small amount of drug may fill void spaces, relieving the packing frustration of the hexagonal phase. However, a higher amount of 1% LAVR-289 induced a modification in the internal structure of hexosomes. This effect is displayed in **Figure 6B**, where $\delta 85$-$\alpha 15$ hexosomes were transformed into an ELP.

Finally, the investigations focused on potential structural modifications induced by the drug when it is incorporated into samples at $\delta 70$ and $\delta 85$-$\alpha 0$ (**Figure 6C**). The incorporation of 0.1% LAVR-289 did not change the mesophase type but led to a reduction in the characteristic distance, as the broad peaks shifted to larger q values in both cases. This effect was similar to that of MCT previously discussed. This observation was consistent with the transition from the hexagonal phase to the L_2 phase observed at $\delta 85$-$\alpha 15$ above a certain content of LAVR-289 (**Figure 6B**). Thus, LAVR-289 can be efficiently incorporated into hexosomes and ELPs at low concentrations (up to 1%) without significantly altering the mesophase structures.
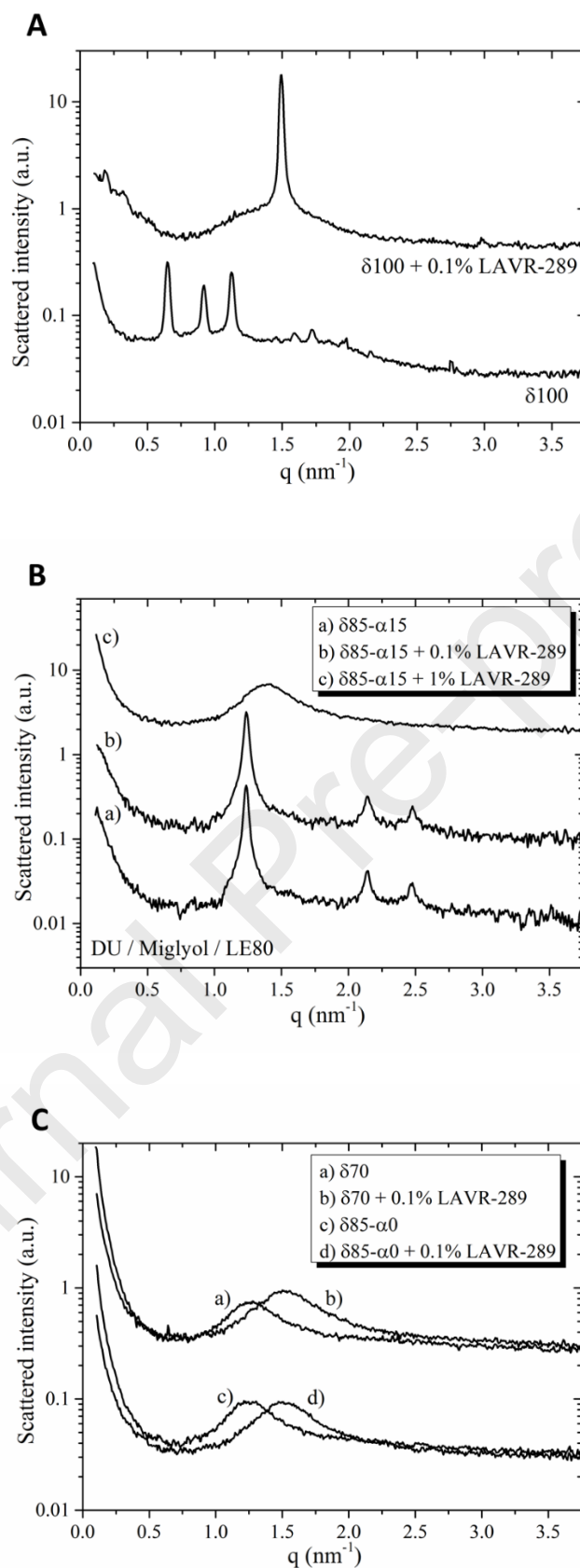
Figure 6: ***A.*** *Effect of 0.1% of LAVR-289 on the scattering curve of a $\delta100$ formulation.* ***B.*** *Effect of LAVR-289 content on the scattering curve of a DU/MCT/LE80 dispersion ($\delta85$-$\alpha15$).* ***C.*** *Effect of 0.1% of LAVR-289 on the scattering curve of DU/MCT EMEs ($\delta70$ and 85).*

3.5. DOSY-NMR *results*

DOSY NMR is a powerful tool for elucidating intermolecular interactions and has gained attention for studying the encapsulation of bioactive drugs within delivery systems.[31] For a considerable period, the oily phase of nanosystems precluded the use of such analysis on these vehicles. However, ongoing improvements in spectrometer sensitivity now enable their utilization. Consequently, DOSY can confirm the encapsulation of a molecule of interest in the dispersed phase environment. A δ85-α15 dispersion was selected as a model for evaluating LAVR-289 encapsulation.

First, ^{1}H spectra of LAVR-289 and blank emulsion spectra were acquired to serve as references (**Figure 7**). Protons of LAVR-289 with chemical shifts distinct from those of the unloaded dispersions were identified at 2.7 ppm and 2.0 ppm. Other signals exhibited chemical shifts similar to those of poloxamer or glyceride compounds. Protons from the acetate functional group and those in the α position of the phosphorus atom, isolated from the rest of the emulsion composition, were used as controls to highlight the proper encapsulation of the lipophilic molecule. It should be noted that loaded and unloaded systems could display different spectra due to interactions between the lipophilic environments and the antiviral molecule.

The 2D DOSY map revealed a main element attributed to the internal oily droplets, evidenced by correlations with the displacement of lipidic protons (0.5 – 1.5 ppm). Correlation peaks with the isolated LAVR-289 protons were identified at the same diffusion coefficient, confirming its successful solubilization in the oily droplets. The sprawl correlation tasks resulted in slight variations in droplet size. For better visibility, an enlargement of the acquisition around the diffusion of the oily phase is presented in **Figure 8**. Dilution of the aqueous phase was necessary to increase spectrum intensity and observe correlations, thereby saturating oily phase-related correlations. This portion of the spectrum is accessible in the supplementary information (**Figure S3**).
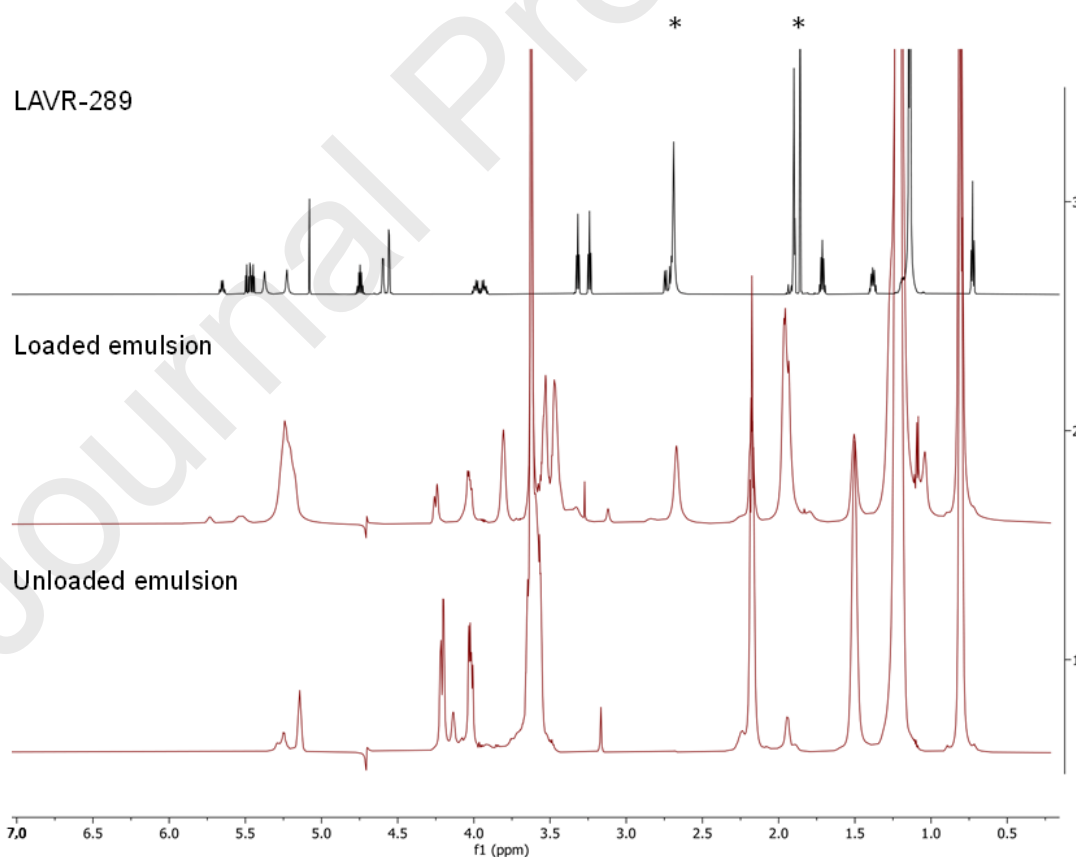

Figure 7: LAVR-289, drug-loaded, and unloaded emulsions ^{1}H-NMR spectra. (represent the signals followed within the loaded emulsions).*
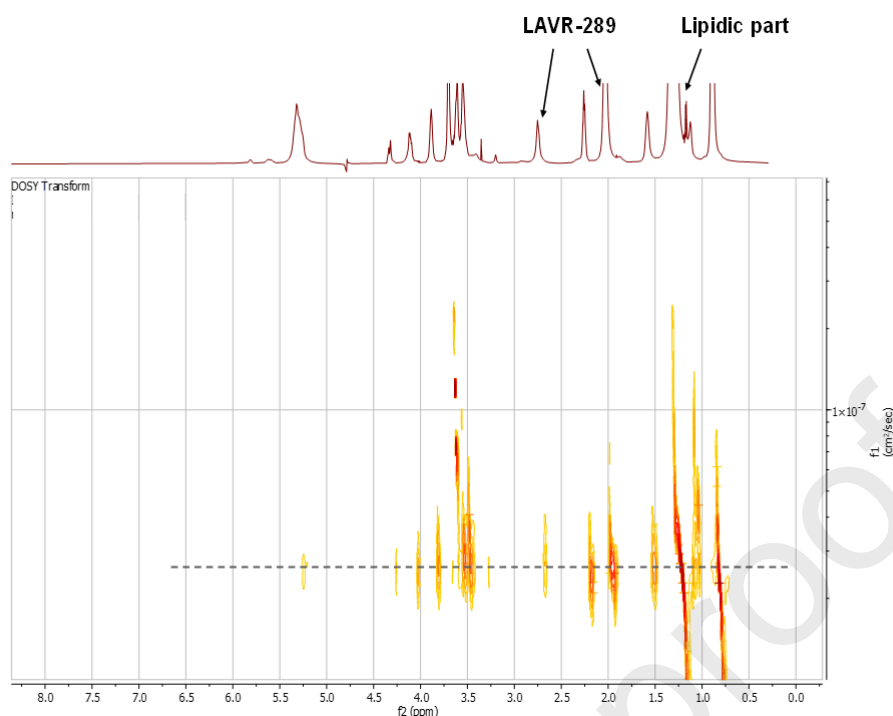
Figure 8: 2D DOSY map of the LAVR-289 loaded emulsion. The spectrum shown in the vertical projection is enlarged to allow better visualization of the resonance's peaks.

3.6. Mesophase dispersions' granulometric profiles and stability

The particle size and distribution of all systems were evaluated to identify the most effective ones. Systems with different lipid ratios, with or without the antiviral drug, showed similar granulometric profiles, suitable for cellular uptake and targeted pharmaceutical applications. An exception was observed in the δ100 system. When LAVR-289 was mixed with the DU/water system (δ100), the cubic bilayer structure completely transformed into a multilamellar structure, presenting significant polydispersity, as discussed in section 3.4. **Figure 6A** depicts the lamellar structure, and **Table S4** lists the data on the larger size and distribution induced.

For emulsions with α-ratio ranging from α0 to α25, granulometric profiles remained comparable, with mean droplet diameters around 280 nm for unloaded mixtures and 250 nm for drug-loaded ones. In all compositions containing LE80, the particle size decreased in the presence of the antiviral, indicating an interaction with the internal emulsion compositions. Beyond α50, the emulsification process became challenging, resulting in larger particles and broader size distributions. At α75, these systems exhibited increased polydispersity and instability over time, with the lipid component quickly flocculating.

The ζ-potential values were also investigated, revealing negative values. These data suggested that the nano-objects could be intrinsically biocompatible as they are less toxic than positively charged nanosystems.[32] Unloaded systems exhibited values around –40 mV, while drug-loaded emulsions showed values of approximately –25 mV. The negative values resulted from partially negatively charged free fatty acids from DU and phosphates from LE80, likely present on the external surfaces of the droplets. The increase in ζ-potential values can be attributed to the partial charging of LAVR-289 on its *N*-heterocyclic moiety at the systems' pH (**Figure S4**), thereby influencing sufficient electrical repulsive forces between the globules.[33]

After three months of storage at 4 °C, all systems exhibited a slight increase in particle size but maintained stability. However, the α0 mixture showed a drastic increase in its polydispersity index. The addition of LE80 not only modulated the mesophase but also enhanced stability to a certain extent. It should be noted that the α50 system (**Table S5**) exhibited macroscopic instability, indicating that excessive amounts of LE80 did not sustain improved stability. Therefore, the presented values are indicative only, as larger clusters could

13

not be detected due to the instrument's analysis range. Furthermore, the pH values measured for the emulsions are compatible with intravenous administration or topical applications. **Table 2** summarizes the characteristics of the LLC selected for *in-cellulo* biological evaluation based on their internal structures. Among these formulations of interest, α15 was used as a model for DOSY-NMR and HPLC studies.

Table 2: Physico-chemical characteristics of emulsions selected for biological evaluations. UL = Unloaded; L = loaded.

Composition		Time	Droplet mean diameter (nm)	PdI	pH
"Unstructured literature - based composition"	**UL**	*t0*	180.1 ± 3.0	0.194	6.7
		3 months	177.0 ± 3.6	0.193	
	L	*t0*	134.7± 4.1	0.223	6.7
		3 months	131.6 ± 4.6	0.219	
δ 85 α0	**UL**	*t0*	271.1 ± 8.1	0.211	6.8
		3 months	299.7 ± 9.3	0.392	
	L	*t0*	230.7 ± 13.2	0.158	6.6
		3 months	267.4 ± 16.7	0.498	
δ 85 α5	**UL**	*t0*	279.1 ± 4.0	0.173	7.1
		3 months	323.2 ± 3.7	0.276	
	L	*t0*	250.9 ± 0.9	0.158	7.0
		3 months	294.1 ± 1.6	0.300	
δ 85 α10	**UL**	*t0*	274.2 ± 8.8	0.231	7.1
		3 months	298.7 ± 7.0	0.245	
		t0	252.5 ± 3.0	0.217	6.9

L	*3 months*	285.4 ± 5.5	0.279	
	t0	264.6 ± 4.2	0.212	
UL				6.8
	3 months	274.5 ± 5.6	0.231	
δ 85 α15				
	t0	265.7 ± 3.3	0.229	
L				6.5
	3 months	258.5 ± 4.8	0.264	
	t0	287.7 ± 4.0	0.243	
UL				6.8
	3 months	304.7 ± 4.2	0.248	
δ 85 α25				
	t0	257.5 ± 2.6	0.225	
L				6.6
	3 months	294.7 ± 3.5	0.323	

Although lipid mesophase dispersions are known for their stability and ability to protect the sensitive molecules incorporated within them, the internal structure was monitored over 8 weeks. To assess the stability of lipidic systems, SAXS measurements of cubosomes (δ100) were conducted throughout this timeframe. The different profiles at various times are presented in the Supporting Information (**Figure S5**). These data showed no significant change in the internal structure over time, as evidenced by consistent plots, confirming the stability of the lipid components. Consequently, the various constituents of these LLC emulsions did not undergo any significant degradation. If there had been any change in the chemical structures of these constituents, it would have resulted in an evolution of the SAXS profile, indicating structural changes in the mesophase through the detection of different types of structures and shifts in peaks.

3.7. Antiviral stability

Since that the emulsification process involved an ultrasonication step, there was a potential risk of active compound degradation. However, several factors ruled out this possibility. Firstly, the molecule endured sonication during its synthesis.[4] Secondly, HPLC analysis could verify the presence or absence of degradation products. For this analysis, unloaded dispersions were injected into the HPLC system as controls after a 1/10 dilution in THF to solubilize all components. This step helped identify peaks resulting from the dispersion components. Subsequently, drug-loaded dispersions underwent the same process and were injected. Dispersions at α0 and α15 served as models.

The resulting chromatograms, displayed in **Figure 9**, show the presence of LAVR-289 at a retention time of 9.5 minutes, for the drug-loaded compositions, with lipid components appearing at the beginning of the chromatograms. No additional chromatographic peaks, unrelated to the dispersion components, were observed. These results confirmed the integrity of the encapsulated antiviral following the emulsification process and demonstrated the bioactive compound's stability over time, even after 3 months of storage at 4°C.
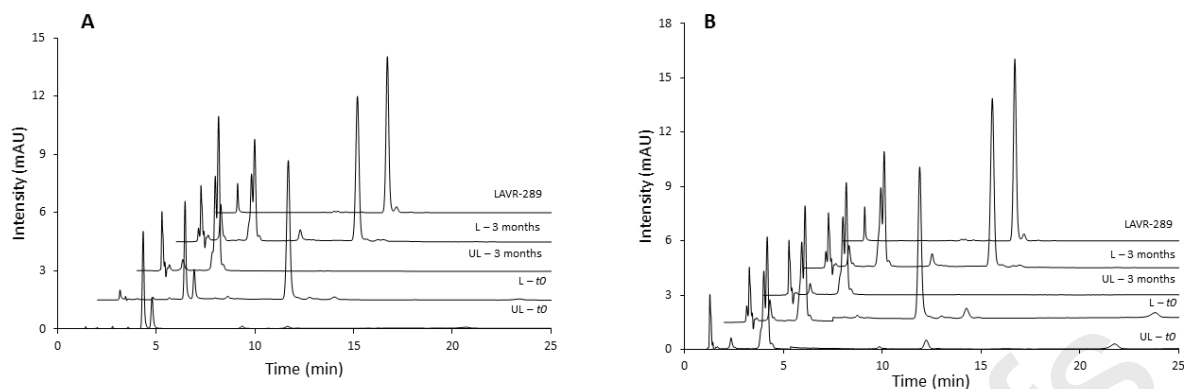
15

*Figure 9: HPLC chromatograms at 267 nm of α0 (**A**) and α15 (**B**) mixtures at t0 and 3 months after production, compared to the LAVR-289 injection. HPLC chromatograms were shifted for better visibility. UL = Unloaded, L = Loaded.*

These results are confirmed by the non-detection of main LAVR degradation product in HPLC chromatograms. Indeed, no peak absorbing at 230 nm appears at the retention time of this degradation product, at 19.1 min, on any of injected samples chromatograms (α0 and α15) after 3 months at 4°C (**Figure S6**).

3.8. *Evaluation of the mesophase dispersions cell viability*

The drug delivery systems were evaluated *in vitro* on HeLa cells infected with the vaccinia virus (VACV). VACV was chosen as a model since it is a recognized mimetic of highly pathogenic poxviruses such as monkeypox or smallpox,[34,35] which have caused several human outbreaks.[36] The dispersion containing DU/MCT did not induce significant cytotoxicity at any tested drug concentrations. However, formulations containing LE80 at concentration of α5 to α20 in the δ85 system showed cytotoxicity 48 hours after treatment for both drug-loaded (10 μM) and unloaded formulations (**Figure 10A**).

This observed cytotoxicity could be due to two factors. First, LAVR-289 solubilized in DMSO at 10 μM reduced cell viability by half after incubation, indicating intrinsic drug cytotoxicity at higher concentrations. When encapsulated within the L_2 mesophase, LAVR-289 did not display intrinsic cytotoxicity. However, cytotoxicity was detected when the drug was formulated within a hexagonal phase. The increased LE80 content appeared to reduce expressed cytotoxicity, possibly due to compositional instability. Therefore, cytotoxicity was only observed when the compound was in a stable hexagonal phase. Secondly, the oily-based composition required sufficient dilution to avoid cell smothering. A one-tenth dilution factor in the culture medium was adequate to maintain cell viability for all compositions (**Figure 10B**). Consequently, for comparative purposes, the drug-loaded concentration was set at 1 μM.
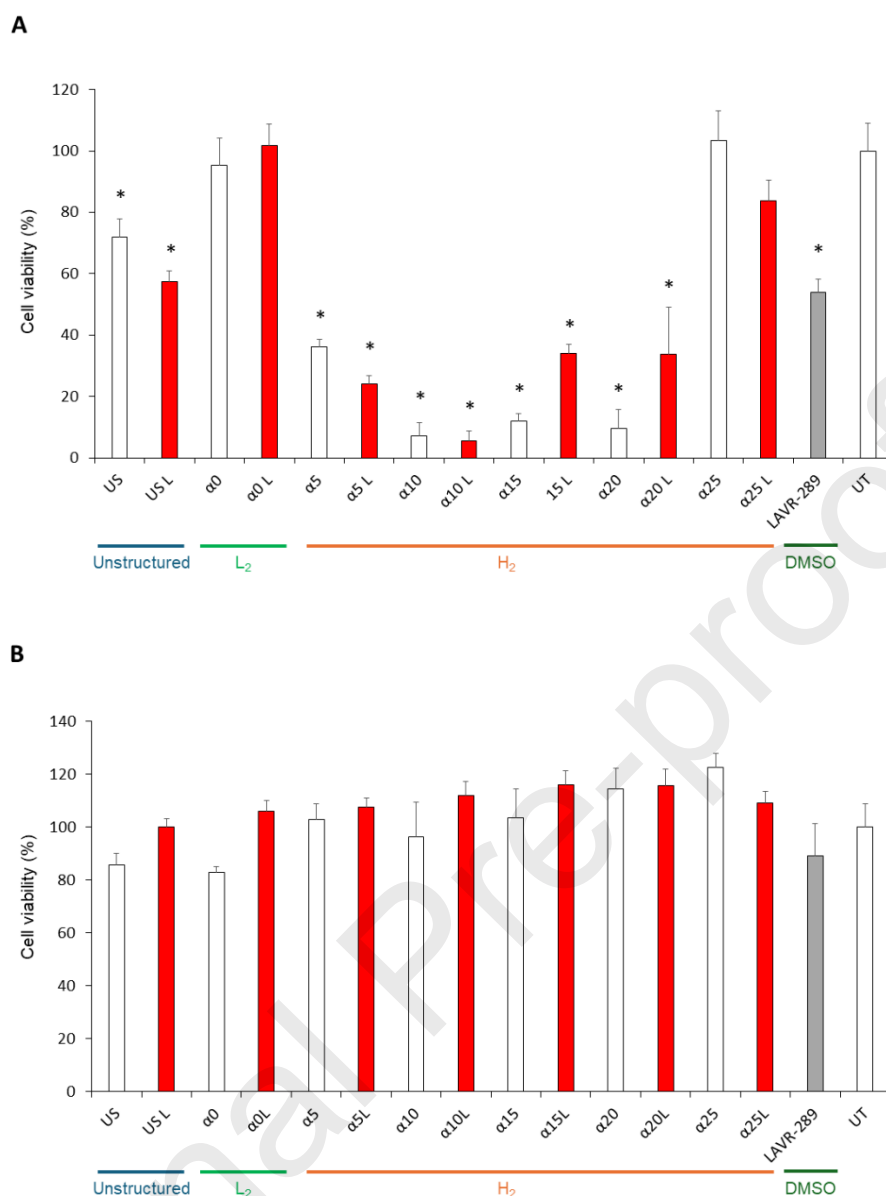
16

A

B

*Figure 10: Cell viability at 10 µM (**A**) and at 1 µM (**B**) of unloaded (white) and drug-loaded systems (red) compared to UT untreated cells. US = Unstructured reference. L = Loaded. * p < 0.05.*

3.9. In-vitro antiviral activity evaluation on HeLa cells

The antiviral efficacy of LAVR-289-loaded mesophase dispersions was assessed on HeLa cells infected with the vaccinia virus. Infection rates were measured 48 hours post-treatment. The results highlighted the strong efficacy of loaded systems compared to their unloaded controls in reducing the propagation of infection, as evidenced by a significant drop in the VACV infection rate (**Figure 11**).

To evaluate the efficiency of different conditions, HeLa cells were stained with Hoechst to visualize their DNA and mark the fixed living cells. VACV ANCHOR™ was used to infect the cells, facilitating the visualization of viral infection and replication. Comparisons were made between uninfected cells, infected untreated cells, and infected treated cells based on these parameters (**Figure 12**). The α15 dispersion served as an illustrative model. At 48 hours post-treatment, the infected treated cells did not exhibit cytotoxicity, and the α15 dispersion significantly inhibited the infection. At α0, the loaded formulation halved the number

17

of VACV-infected cells. At $\alpha 5$ this rate was reduced by a factor of seven, reflecting a sharp decrease in the rate of infected cells at the L_2/H_2 structural transition, highlighting the effect of internal structure on antiviral activity. Thus, the slight addition of LE80 to the delivery system composition to induce the phase transition reduced the percentage of infected cells.

The observed activity variation is consistent with previous research, where internal mesophase structures are known to impact the release rate of encapsulated drugs, influencing both bioavailability and therapeutic efficacy.[37,38] Non-lamellar phases, particularly hexagonal phases, have been shown to significantly enhance the cellular penetration of hydrophobic drugs by at least twofold.[39] This enhanced penetration is likely due to increased uptake efficiency, as non-lamellar LLCs are believed to be internalized via multiple mechanisms. Regarding non-lamellar LLCs, the cellular penetration may vary due to differing physicochemical properties. The L_2 phase is more fluid, while the H_2 phase exhibits a more gel-like consistency and a more complex structure. These differences may result in distinct internalization processes between the phases, thereby influencing the activity of the solubilized drug. Consequently, the superior activity observed for the hexagonal phase at $\alpha 5$ can be attributed to a more efficient internalization process compared to unstructured or disordered micellar phases resulting from a structural-based cell penetration impact. This concept is a key focus in current drug delivery research, with cubosomes potentially offering superior delivery capabilities compared to other systems.[40] However, in our case, this phase could not be stabilized for comparison.

In the H_2 mesophase part, increasing the LE80 content (and thus the α rate) initially maintained antiviral activity but became progressively less effective, with activity at $\alpha 25$ resembling that of $\alpha 0$. This rise in LE80 induced internal structural changes due to a less negative mean curvature at the hydrophobic/hydrophilic interfaces. Consequently, the expansion of water channel diameters, as evidenced by the enlarged lattice parameters in **Figure 5**, increased the water domains proportion inside the particles. As previously reported, the proportion of aqueous/lipophilic domains play a critical role in drug diffusion within the particles.[41] Given LAVR-289's hydrophobicity, the increased water channels volume may hinder its diffusion within the particle, thereby reducing its activity.

In comparison, the evaluation of free LAVR-289 solubilized in DSMO demonstrated enhanced antiviral activity. This improvement can be attributed to the significant effect of the solvent on cellular penetration. Specifically, DMSO has the capability to disrupt the lipid bilayer, thereby reducing natural barrier resistance and facilitating the penetration of the solubilized drug. Despite DMSO's unsuitability for *in-vivo* use, this suggests that not all encapsulated antiviral agents within the LLC were fully released, thereby supporting the sustained release nature of these systems.

Therefore, optimal efficacy was observed at compositions around $\alpha 5$-$\alpha 10$, as a too-slow release is not desired to achieve antiviral activity. The decrease in antiviral activity with increased LE80 quantity showed that efficiency was not solely related to the surfactant ratio but also to the effect of the hexagonal structure. This slight loss of activity could be correlated with the formulation's compositions. The best antiviral activity was observed for optimization considering the best mesophase and the ability to be formulated. Excessive LE80 ($\alpha \geq 25$) destabilized the systems, leading to a decrease in antiviral activity. Additionally, for all compositions, higher dilutions (0.1 μM or 0.01 μM) did not maintain antiviral activity over the study period.
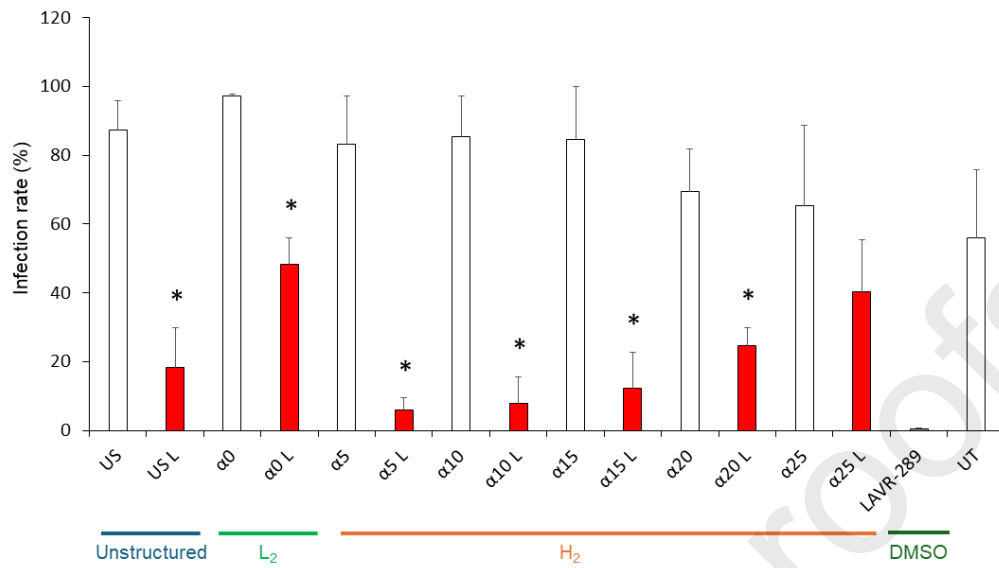
*Figure 11: Loaded mesophase dispersions effectively reduce cells infection after 48 hours. * p<0.05 compared with their unloaded mixtures at the same α ratio.US = Unstructured reference; L = Loaded.*
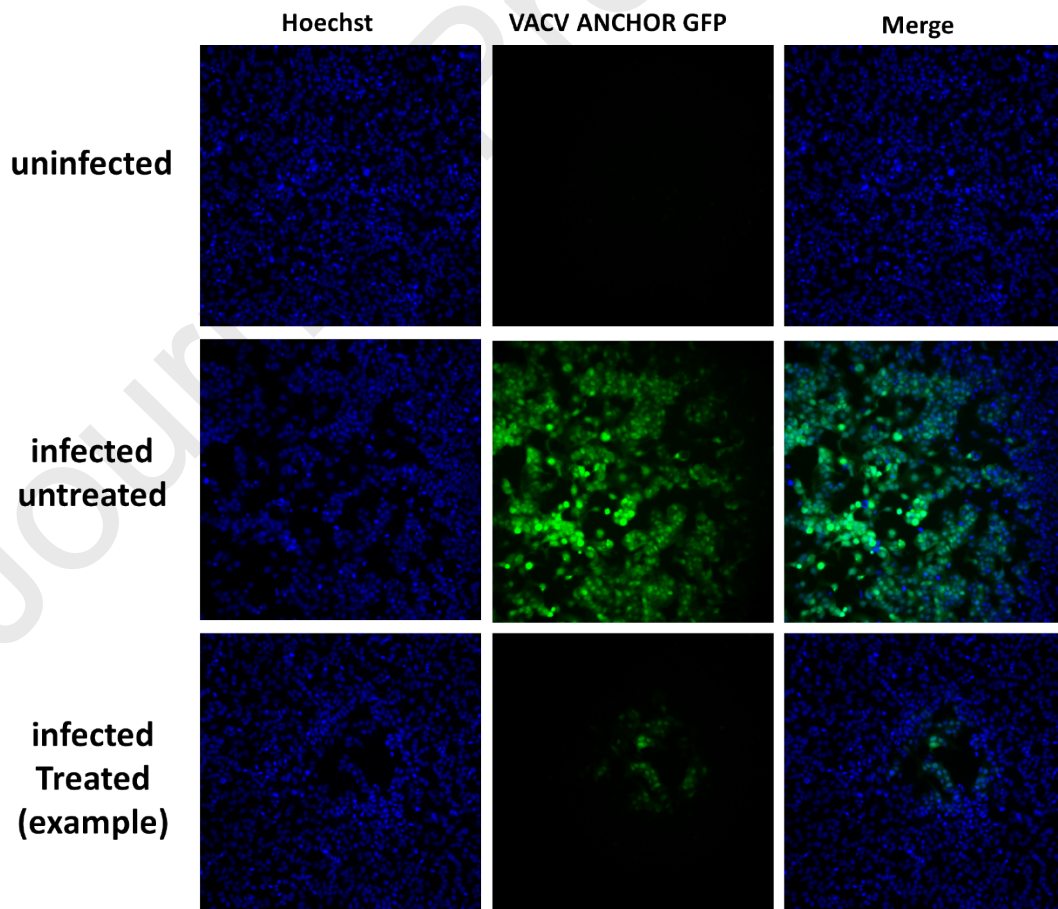
Figure 12: Illustration of living cells (Hoechst staining) and infection (VACV Anchor GFP) for uninfected, infected untreated, and infected α15 treated conditions.

These results emphasized the significant impact of mesophases on the antiviral activity of lipophilic drugs. Hexosomes, compared to ELPs or unstructured emulsions, showed superior antiviral activity against VACV-infected cells with an optimized MCT-LE80 ratio. At 1 μM of LAVR-289, viral infection was reduced by up to 95%, confirming the potential of hexosomes in delivering optimized antiviral therapy.

4. Conclusions

Lipidic nanosystems, particularly lyotropic liquid crystalline structures, offer promising solutions for encapsulating, protecting, and delivering new drug candidates or enhancing the bioavailability and efficacy of commercialized active pharmaceutical ingredients. These drug delivery systems are especially beneficial for hydrophobic drugs, like antiviral prodrugs, helping to overcome limitations in their development. LAVR-289, a new ANP antiviral with significant lipophilicity indicated by a high LogP value, was selected for pre-clinical study development. The goal was to create biocompatible, biodegradable, FDA-approved systems suitable for oral, topical, or intravenous administrations. Various mesophase dispersions, optimized through careful modulation of emulsifiers, were designed for the administration of LAVR-289. At 1 μM LAVR-289, dispersed systems significantly reduced infection rates 48 hours after contact without cytotoxicity. The internal mesophase and composition are found to influence the biological results, and among formulations, hexosomes with not too large LE80 amounts demonstrated superior antiviral efficacy against *in vitro* vaccinia virus-infected cells. The findings underscore the potential of tailored mesophase dispersions for enhancing the delivery and efficacy of lipophilic antiviral drugs like LAVR-289. Further optimization and detailed mechanistic studies are warranted to fully exploit these systems for clinical applications. The results provide a promising foundation for developing advanced drug delivery vehicles that leverage mesophase structures to improve therapeutic outcomes.

5. Author contributions

M.B.: Conceptualization, Methodology, Investigation, Formal analysis, Visualization, Writing – Original Draft & Editing. **T.M.:** LogP Investigation, Formal analysis. **S.G.:** Conceptualization, Methodology, Formal analysis, Writing – Original Draft. **F.M.:** Conceptualization, Methodology. **V.R.:** Resources, Funding acquisition. **E.M.:** *In-vitro* Investigation. **F.G.:** *In-vitro* Investigation. **F.C.M.:** Resources. **P.F.:** Conceptualization, Writing – Review. **L.A.A.:** Resources, Funding acquisition.

6. Additional information

The authors declare that the research was conducted without any commercial or financial relationships that could be construed as a potential conflict of interest. F.G. and E.M. are shareholder and employee of NeoVirTech, respectively.

7. Supporting information available

Supplementary SAXS, granulometric data, LogP graph, aqueous phase DOSY-NMR spectra, and evolution of protonated LAVR-289 forms as a function of pH are available in the supporting information.

8. Acknowledgments

9. References

[1] Khan, S., Sharma, A., Jain, V., 2023. An Overview of Nanostructured Lipid Carriers and its Application in Drug Delivery through Different Routes. Adv. Pharm. Bull. 13, 446-460. https://doi.org/10.34172/apb.2023.056.

[2] Anselmo, A.C., Mitragotri, S., 2021. Nanoparticles in the clinic: An update post COVID-19 vaccines. Bioeng. Transl. Med. 63, e10246. https://doi.org/10.1002/btm2.10246.

[3] Delshadi, R., Bahrami, A., McClements, D.J., Moore, M.D., Williams, L., 2021. Development of nanoparticle-delivery systems for antiviral agents: A review. J. Control. Release. 331, 30-44. https://doi.org/10.1016/j.jconrel.2021.01.017.

[4] Bessières, M., Roy, V., Abuduani, T., Favetta, P., Snoeck, R., Andrei, G., Moffat, J., Gallardo, F., Agrofoglio, L.A., 2024. Synthesis of LAVR-289, a new [(Z)-3-(acetoxymethyl)-4-(2,4-diaminopyrimidin-6-yl)oxy-but-2-enyl]phosphonic acid prodrug with pronounced antiviral activity against DNA viruses. Eur. J. Med. Chem. 271:116412. https://doi.org/10.1016/j.ejmech.2024.116412.

[5] Chen, R., Wang, T., Song, J., Pu, D., He, D., Li, J., Yang, J., Li, K., Zhong, C., Zhang, J., 2021. Antiviral Drug Delivery System for Enhanced Bioactivity, Better Metabolism and Pharmacokinetic Characteristics. Int. J. Nanomedicine. 16, 4959-4984. https://doi.org/10.2147/IJN.S315705.

[6] Cojocaru, F.D., Botezat, D., Gardikiotis, I., Uritu, C.M., Dodi, G., Trandafir, L., Rezus, C., Rezus, E., Tamba, B.I., Mihai, C.T., 2020. Nanomaterials Designed for Antiviral Drug Delivery Transport across Biological Barriers. Pharmaceutics. 12, 171-204. https://doi.org/10.3390/pharmaceutics12020171.

[7] Amidon, G. L.; Lennernäs, H.; Shah, V. P.; Crison, J. R.,1995. A Theoretical Basis for a Biopharmaceutic Drug Classification: The Correlation of in Vitro Drug Product Dissolution and in Vivo Bioavailability. Pharm. Res. 12, 413–420. https://doi.org/10.1023/A:1016212804288.

[8] Preeti, Sambhakar, S., Saharan, R., Narwal, S., Malik, R., Gahlot, V., Khalid, A., Najmi, A., Zoghebi, K., Halawi, M. A., Albratty, M., Mohan, S., 2023. Exploring LIPIDs for their potential to improves bioavailability of lipophilic drugs candidates: A review. Saudi Pharm. J. 31, 101870. https://doi.org/10.1016/j.jsps.2023.101870.

[9] Chountoulesi, M., Pispas, S., Tseti, I.K., Demetzos, C., 2022. Lyotropic Liquid Crystalline Nanostructures as Drug Delivery Systems and Vaccine Platforms. Pharmaceuticals. 15, 429. https://doi.org/10.3390/ph15040429.

[10] Blanco-Fernández, G., Blanco-Fernández, B., Fernández-Ferreiro, A., Otero-Espinar, F. J., 2023. Lipidic lyotropic liquid crystals: Insights on biomedical applications. Adv. Colloid Interface Sci. 313, 102867. https://doi.org/10.1016/j.cis.2023.102867.

[11] Dinh, L., Yan, B., 2023. Oral Drug Delivery via Intestinal Lymphatic Transport Utilizing Lipid-Based Lyotropic Liquid Crystals. Liquids. 3, 456-468. https://doi.org/10.3390/liquids3040029.

[12] Priya, S., Desai, V.M., Singhvi, G., 2024. Tailoring lyotropic liquid crystals for skin barrier penetration: Exploring composition and structure–function relationships. Appl. Phys. Rev. 11, 3, 031307. https://doi.org/10.1063/5.0204909.

[13] Piorkowski, D. T., McClements, D. J., 2014. Beverage Emulsions: Recent Developments in Formulation, Production, and Applications. Food Hydrocoll. 42, 5−41. https://doi.org/10.1016/j.foodhyd.2013.07.009.

[14] Chavda, V.P., Dyawanapelly, S., Dawre, S., Ferreira-Faria, I., Bezbaruah, R., Rani Gogoi, N., Kolimi, P., Dave, D.J., Paiva-Santos, A.C., Vora, L.K., 2023. Lyotropic liquid crystalline phases: Drug delivery and biomedical applications. Int. J. Pharm. 647, 123546. https://doi.org/10.1016/j.ijpharm.2023.123546.

[15] Chavda, V.P., Dawre, S., Pandya, A., Vora, L.K., Modh, D.H., Shah, V., Dave, D.J., Patravale, V., 2022. Lyotropic liquid crystals for parenteral drug delivery. J. Control. Release. 349, 533-549. https://doi.org/10.1016/j.jconrel.2022.06.062.

[16] Gustafsson, J., Ljusberg-Wahren, H., Almgren, M., Larsson, K., 1996. Cubic lipid water phase dispersed into submicron particles. Langmuir. 12, 4611–4613. https://doi.org/10.1021/la960318y.

[17] Barauskas, J., Johnsson, M., Tiberg, F., 2005. Self-Assembled Lipid Superstructures: Beyond Vesicles and Liposomes. Nano Lett. 5, 1615–1619. https://doi.org/10.1021/nl050678i.

[18] Gustafsson, J., Ljusberg-Wahren, H., Almgren, M., Larsson, K., 1997. Submicron particles of reversed lipid phases in water stabilized by a nonionic amphiphilic polymer. Langmuir. 13, 6964–6971. https://doi.org/10.1021/la970566+.

[19] Yaghmur, A., de Campo, L., Salentinig, S., Sagalowicz, L., Leser, M.E., Glatter, O., 2006. Oil-loaded monolinolein-based particles with confined inverse discontinuous cubic structure (Fd3m). Langmuir. 22, 517–521. https://doi.org/10.1021/la052109w.

[20] Pilman, E., Larsson, K., Tornberg, E., 1980. Inverse micellar phases in ternary systems of polar lipids/fat/water and protein emulsification of such phases to w/o/w microemulsion-emulsions. J. Dispers. Sci. Technol. 1, 267–281. https://doi.org/10.1080/01932698008962171.

[21] Yaghmur, A., de Campo, L., Sagalowicz, L., Leser, M.E., Glatter, O., 2005. Emulsified microemulsions and oil-containing liquid crystalline phases. Langmuir. 21, 569-577. https://doi.org/10.1021/la0482711.

[22] Guillot, S., Méducin, F., Poljak, K., Mallard, V., Foucault, A., Serieye, S., Pichon, C., 2017. Nanostructured monolinolein miniemulsions as delivery systems: role of the internal mesophase on cytotoxicity and cell internalization. Int. J. Pharm. 523, 142-150. https://doi.org/10.1016/j.ijpharm.2017.03.012.

[23] Huang, Y., Gui, S., 2018. Factors affecting the structure of lyotropic liquid crystals and the correlation between structure and drug diffusion. RSC Adv. 8, 6978-6987. https://doi.org/10.1039/C7RA12008G.

[24] Pradère, U., Clavier, H., Roy, V., Nolan, S.P., Agrofoglio, L.A., 2011. The shortest strategy for generating phosphonate prodrugs by olefin cross-metathesis – Application to acyclonucleoside phosphonates. Eur. J. Org. Chem. 36, 7324-7330. https://doi.org/10.1002/ejoc.201101111.

[25] OCDE (2022), Test No. 117: Partition Coefficient (n-octanol/water), HPLC Method, OECD Guidelines for the Testing of Chemicals, Section 1, Éditions OCDE, Paris, https://doi.org/10.1787/9789264069824-en.

[26] De Campo, L., Yaghmur, A., Sagalowicz, L., Leser, M. E., Watzke, H., Glatter, O., 2004. Reversible Phase Transitions in Emulsified Nanostructured Lipid Systems. Langmuir. 20, 5254–5261. https://doi.org/10.1021/la0499416.

[27] Prévot, G., Soria, F.N., Thiolat, M.L., Daniel, J., Verlhac, J.B., Blanchard-Desce, M., Bezard, E., Barthélémy, P., Crauste-Manciet, S., Dehay, B., 2018. Harnessing Lysosomal pH through PLGA Nanoemulsion as a Treatment of Lysosomal-Related Neurodegenerative Diseases. Bioconjug. Chem. 29, 4083-4089. https://doi.org/10.1021/acs.bioconjchem.8b00697.

[28] Brouillard, M., Kinet, R., Joyeux, M., Dehay, B., Crauste-Manciet, S., Desvergnes, V., 2023. Modulating Lysosomal pH through Innovative Multimerized Succinic Acid-Based Nucleolipid Derivatives. Bioconjug. Chem. 34, 572-580. https://doi.org/10.1021/acs.bioconjchem.3c00041.

[29] IOI MIGLYOL® 812 N & IMWITOR® 742 PRODUCT SPOTLIGHTS. Accessed 30 July 2024. Available from: https://www.ioioleo.de/wp-content/uploads/2024/07/IOI_Spotlights_Pharma_WEB.pdf.

[30] Sagalowicz, L., Guillot, S., Acquistapace, S., Schmitt, B., Maurer, M., Yaghmur, A., de Campo, L., Rouvet, M., Leser, M., Glatter, O., 2013. Influence of Vitamin E Acetate and Other Lipids on the Phase Behavior of Mesophases Based on Unsaturated Monoglycerides. Langmuir. 29, 8222−8232. https://doi.org/10.1021/la305052q.

[31] Pagès, G., Gilard, V., Matinob, R., Malet-Martino, M., 2017. Pulsed-field gradient nuclear magnetic resonance measurements (PFG NMR) for diffusion ordered spectroscopy (DOSY) mapping. Analyst. 142, 3771-3796. https://doi.org/10.1039/C7AN01031A

[32] Shao, X. R., Wei, X. Q., Song, X., Hao, L. Y., Cai, X. X., Zhang, Z. R., Peng, Q., Lin, Y.F., 2015. Independent effect of polymeric nanoparticle zeta potential/surface charge, on their cytotoxicity and affinity to cells. Cell Prolif. 48, 465-474. https://doi.org/10.1111/cpr.12192

[33] Washington, C., Chawla, A., Christy, N., Davis, S.S., 1989. The electrokinetic properties of phospholipid-stabilized fat emulsions. Int. J. Pharm. 54, 191–7. https://doi.org/10.1016/0378-5173(89)90096-3.

[34] Thèves, C., Crubézy, E., Biagini, P., 2016. History of Smallpox and Its Spread in Human Populations. Microbiol. Spectr., 4. https://doi.org/10.1128/microbiolspec.poh-0004-2014.

[35] McFadden, G., 2005. Poxvirus tropism. Nat. Rev. Microbiol. 3, 201-13. https://doi.org/10.1038/nrmicro1099.

[36] El-Jesr, M., Teir, M., Maluquer de Motes, C., 2020. Vaccinia Virus Activation and Antagonism of Cytosolic DNA Sensing. Front. Immunol. 11:568412. https://doi.org/10.3389/fimmu.2020.568412.

[37] Chen, Y., Ma, P., Gui, S., 2014. Cubic and Hexagonal Liquid Crystals as Drug Delivery Systems. Biomed. Res. Int. 815981. http://dx.doi.org/10.1155/2014/815981.

[38] Mo, J., Milleret, G., Nagaraj, M., 2017. Liquid crystal nanoparticles for commercial drug delivery. Liq. Cryst. Rev. 5, 69–85. https://doi.org/10.1080/21680396.2017.1361874.

[39] Yap, S. L., Yu, H., Li, S., Drummond, C. J., Conn, C. E., Tran, N., 2024. Cell interactions with lipid nanoparticles possessing different internal nanostructures: Liposomes, bicontinuous cubosomes, hexosomes, and discontinuous micellar cubosomes. J. Colloid Interface Sci. 656, 409-423. https://doi.org/10.1016/j.jcis.2023.11.05.

[40] Mohammad, Y., Prentice, R.N., Boyd, B.J., Rizwan, S.B., 2022. Comparison of cubosomes and hexosomes for the delivery of phenytoin to the brain. J. Colloid Interface Sci. 605, 146–154. https://doi.org/10.1016/j.jcis.2021.07.070

[41] Negrini, R., Mezzenga, R., 2012. Diffusion, molecular separation, and drug delivery from lipid mesophases with tunable water channels. Langmuir. 28, 16455-62. https://doi.org/10.1021/la303833s.